frontiers in Chemical Engineering

REVIEW
published: 14 March 2022
doi: 10.3389/fceng.2022.810443

Hierarchical COK-X Materials for Applications in Catalysis and Adsorptive Separation and Controlled Release

*Sreeprasanth Pulinthanathu Sree, Eric Breynaert, Christine E. A. Kirschhock and Johan A. Martens**

Center for Surface Chemistry and Catalysis (COK) KU, Leuven, Belgium

Over the years, COK has developed a family of silicate materials and metal–organic framework hybrids with hierarchical porosity and functionality, coined zeogrids, zeotiles, and COK-x (stemming from the Flemish name of the laboratory "Centrum voor Oppervlaktechemie en Katalyse"). Several of these materials have unique features relevant to heterogeneous catalysis, molecular separation, and controlled release and found applications in the field of green chemistry, environmental protection, and pharmaceutical formulation. Discovery of a new material typically occurs by serendipity, but the research was always guided by hypothesis. This review provides insight in the process of tuning initial research hypotheses to match material properties to specific applications. This review describes the synthesis, structure, properties, and applications of 12 different materials. Some have simple synthesis protocols, facilitating upscaling and reproduction and rendering them attractive also in this respect.

Keywords: zeotiles, zeogrids, COK-12, COK-15, COK-18, COK-19

OPEN ACCESS

Edited by:
Anne Galarneau, UMR5253 Institut de chimie moléculaire et des matériaux Charles Gerhardt Montpellier (ICGM), France

Reviewed by:
Alexander Nikiforov, Lomonosov Moscow State University, Russia
Jean-Pierre Gilson, École Nationale Supérieure d'ingénieurs De Caen, France

****Correspondence:***
Johan A. Martens
johan.martens@kuleuven.be

Specialty section:
This article was submitted to Materials Process Engineering, a section of the journal Frontiers in Chemical Engineering

Received: *07 November 2021*
Accepted: *28 January 2022*
Published: *14 March 2022*

Citation:
Pulinthanathu Sree S, Breynaert E, Kirschhock CEA and Martens JA (2022) Hierarchical COK-X Materials for Applications in Catalysis and Adsorptive Separation and Controlled Release. Front. Chem. Eng. 4:810443. doi: 10.3389/fceng.2022.810443

INTRODUCTION

Pores are an essential feature of materials developed with a focus toward practical applications in which adsorption and chemical conversion of molecules are involved. Pores generate surface area available for molecular interactions, void volume to incorporate hybrid components, and access ports, which can be exploited for molecular sieving. Dimensionwise, pores can be subdivided into micropores (diameters smaller than 2 nm), mesopores (2–50 nm) exhibiting capillary condensation, and macropores (wider than 50 nm) in which fluids assume their bulk behavior. Introduced in the 1960s (Dubinin, 1968), this categorization is still very useful today, especially when treating hierarchical materials where two or three types of pores are combined. Through the years, COK has discovered several materials that are classified as hierarchical and in which the pore architecture contributes special properties. In the field of silicates, we have discovered the "zeotiles" (a pun on the word "zeolites") and "zeogrids," which are hierarchical materials obtained *via* mesoscale structuring of prefabricated zeolitic precursor units called "zeolite nanoslabs." Assembling zeolitic building units in the presence of micellar templates, a pore hierarchy in two and three dimensions was developed.

Metal–organic frameworks (MOFs) is another field where next to porosity, the chemistry of the linkers and the metal nodes of the framework can be adapted, such as to achieve unique selectivity in adsorption and molecular separation. The wealth of chemistry that can be built into these frameworks opens up all possible physical and chemical interactions with guest molecules, much

more than with silicates. Organic as well as inorganic molecular templates are used to favor the polymerization of desired phases and to stabilize them for usage.

OVERVIEW OF MATERIALS AND THEIR APPLICATIONS

Zeogrids and zeotiles

Zeolites with MFI framework topology, especially ZSM-5, are very successful as acid catalysts in hydrocarbon conversion processes. The MFI type framework has two types of intersecting channels, straight and zigzag, and circumscribed with 10-membered rings. By running in two crystallographic orientations, they provide the zeolite with shape-selective properties. ZSM-5 zeolite is used as an additive to ultrastable Y zeolites in fluid catalytic cracking (FCC) processes for both propylene production and gasoline octane improvement (Madon, 1991). In this application, minimization of intracrystalline diffusion limitations is essential. Reducing the distance between bulk liquid and pore, by minimizing crystallite size, explains why the MFI type was one of the first zeolites for which the synthesis of nanosized particles has been reported (Persson et al., 1994; Ravishankar et al., 1998, Ravishankar et al., 1999). Structuring such nanosized crystallites into a macroscopic hierarchical structures with meso, micropores interconnecting the nanosized crystallites represented an even more attractive route to reduce diffusion limitations.

MFI-type zeolites are typically synthesized using tetrapropylammonium cations (TPA) as a structure-directing agent (Flanigen et al., 1978; Kokotailo et al., 1978; Jacobs, 1987). A silica source, tetraethyl orthosilicate (TEOS), when hydrolyzed in the presence of tetrapropylammonum hydroxide (TPAOH) creates a clear sol of nanoparticles called "clear solution" (Schoeman and Regev, 1996). The nature of these nanoparticles is intriguing, and many descriptions have been formulated explaining the interaction of TPA with the embryonic zeolite. Hypothetical sequences of molecular steps leading to encapsulation of a TPA+ molecule in a precursor of a channel intersection of the final zeolite framework have been reported (Burkett and Davis, 1995; Dokter et al., 1995; Kirschhock et al., 1999c; Rimer et al., 2005; Haouas et al., 2009). Once formed, the connectivity of silica in these nanoparticles starts to diverge from oligomers in solution and sequentially reaches the connectivity as observed in MFI (Lesthaeghe et al., 2008; Haouas et al., 2009). Either *via* hydrothermal treatment or by long-term aging at room temperature, the protozeolitic particles enhance their internal ordering to aggregate into zeolite nanoparticles (Kirschhock et al., 1999a; Davis et al., 2006; Aerts et al., 2007; Liang et al., 2007). Transmission electron microscopic (TEM) observation of the nanoparticles evidenced the existence of slab-shaped particles having long dimensions of ca. 4 nm × 4 nm (Kirschhock et al., 2001; Aerts et al., 2003), and atomic force microscopy (AFM) revealed the heights of these slabs to be ca.1.3 nm and its multiples (Ravishankar et al., 1998), explaining the notion of "nanoslab." Nanoslabs, half nanoslabs, tablets, staples of tablets, and MFI zeolite nanocrystallites are created by hydrolyzing TEOS

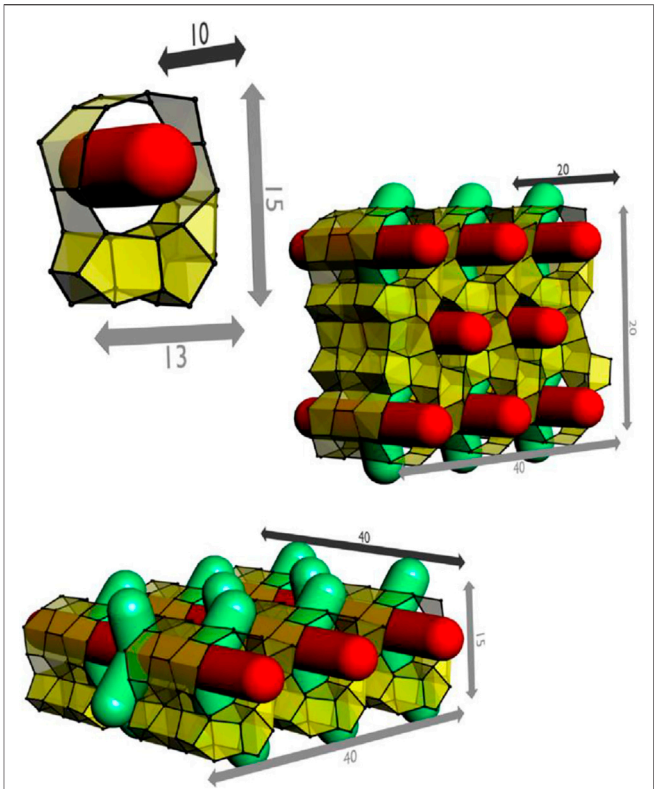

FIGURE 1 | Representation of idealized precursor and two nanoslabs (sizes indicated in Å units). Straight channels are indicated in red, zigzag channels in green (adapted with permission from Martens et al., 2011).

in concentrated TPAOH solution to create protozeolitic particles that aggregate subsequently upon dilution. Heating is needed for growing of larger crystals (Kirschhock et al., 1999b; Ravishankar et al., 1999; Kremer et al., 2005b). Idealized representations of protozeolitic particles (Martens et al., 2011) (**Figure 1**) explaining the NMR spectroscopic fingerprints and the bathochromic shifting of spectroscopic fingerprints, such as the Pentasil IR absorption band at 540–550 cm^{-1} according to the evolution from an isolated five-ring to full embedment in MFI framework (Lesthaeghe et al., 2008). The comparison of molecular simulations and experimental data of IR bands in nanoparticles extracted from silicalite-1 clear solutions supported their structured nature. Although the proposed aggregation has been debated in literature (Kragten et al., 2003; Ramanan et al., 2004), existence of nanoslabs has been a fruitful hypothesis for designing new materials.

Several hierarchical structures have been obtained from nanoslab suspensions by using surfactant templates for ordering their assembly (Kirschhock et al., 2005; Martens et al., 2011). An overview of different types of hierarchical silicate structures realized using this approach is provided in **Table 1**.

Zeogrids were initial synthesis successes of this approach. The name was selected based on the appearance of the structure as an interposed stapling of individual nanoslabs. Zeogrid was

TABLE 1 | Hierarchical silicate materials created using the nanoslab approach.

Material	Micelle template	Pore shape/ diameter (nm)/symmetry	References
Zeogrid	[a]CTAB in EtOH	Slit-like pores/1.4 nm/layered structure	Kremer et al. (2000), Kremer et al. (2002); Kremer et al. (2005b)
Zeotile-1	CTAB aqueous	Hexagonal pores/3.5 nm/triangular pores/1.4 nm/hexagonal	Kremer et al. (2003)
Zeotile-2	CTAB powder	Gyroid/2.7 nm/Cubic	Kremer et al. (2003); Kremer et al. (2005a)
Zeotile-4	[b]Pluronic P123-aqueous	Hexagonal channels: 10 nm slit-like pores: ~3 nm/hexagonal	Kremer et al. (2003); Bals et al. (2009)
Spherical zeotile-4 (3–10 μm)	Pluronic P123 and CTAB	Cylindrical/7 nm/hexagonal	Martens et al. (2011)
Zeotile-4 (P104)	[c]Pluronic P104 aqueous	Cylindrical/11 nm/hexagonal	(Pulinthanathu Sree et al. (2012); Pulinthanathu Sree et al. (2017)
Spherical silica balls (5 μm) (zeotile-4 based)	[d]Pluronic P85 aqueous	Cylindrical/5 nm/unordered	Martens et al. (2011); Pulinthanathu Sree et al. (2012), Pulinthanathu Sree et al. (2017)
Zeotile-6	CTAB powder	Cylindrical/3.8 nm/hexagonal	Martens et al. (2011)
Highly porous films *via* spin coating (zeotile-4 based)	Pluronic P123/ aqueous + ethanol	Cylindrical/6–18 nm/random	Sree et al. (2011)

[a]*CTAB-([(C16H33)N(CH3)3]Br.*
[b]*Pluronic P123-[(EO)20(PO)70(EO)20].*
[c]*Pluronic P104-[(EO)27(PO)61(EO)27]*
[d]*Pluronic P85-[(EO)25(PO)40(EO)25].*

precipitated from the MFI nanoslab suspension by the addition of a saturated ethanolic solution of cetyltrimethylammonium bromide (CTAB) (Kremer et al., 2000, Kremer et al., 2002; Kremer et al., 2005b) In a zeogrid, the nanoparticles self-organize into layers intercalated by surfactant molecules (**Figure 2**). Following calcination to get rid of TPA and CTAB, macroscopic white particles exhibiting a dual microporosity are obtained. One type of micropore *viz.* ultramicropore (0.7 nm<) arises from inside the nanoslabs and the other one, which is supermicropore (>0.7 nm), is a result of spacing between the slab layers in between individual blocks leaving an opening. By modeling the N_2 adsorption isotherms, the height of these spacings was estimated as ca. 1.4 nm, which is comparable with the thickness of an individual height of nanoslabs (Aerts et al., 2003; Aerts et al., 2004).

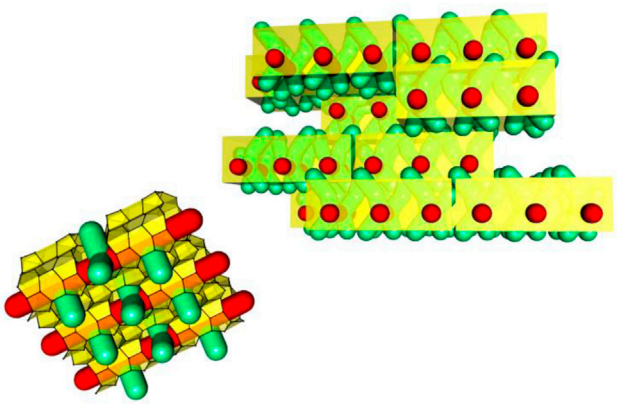

FIGURE 2 | Schematic representation of tiling patterns of nanoslabs in a zeogrid (adapted with permission from Martens et al., 2011).

The molecular sieving properties of zeogrids were revealed with pulse gas chromatographic separation of alkane mixtures. Preferential adsorption of n-octane over isooctane confirmed the presence molecular shape selectivity being characteristic of ultramicropores (Kremer et al., 2002). Traditional MFI zeolites separate branched alkanes from linear ones regardless of the carbon number. Zeogrids behave differently. When the branched alkane is heavier than the linear one, the branched isomer is preferentially adsorbed. This deviation from the behavior of an MFI zeolite has been ascribed to the supermicropores. Ultramicropores can differentiate molecules based on their molecular weight, while supermicropores do this based on branchiness. Zeogrid offers the possibility to tune the adsorption preferences by altering the size of the building blocks, thus, tuning the size of the supermicropores to obtain the desired property (Kremer et al., 2002).

The molecular separation potential of Zeogrids was also revealed turning them into membranes (Martens et al., 2011). Continuous zeogrid layers were prepared by dipcoating nanoslab suspensions on flat and tubular porous alumina supports. Single gas measurements of N_2, H_2, and CO_2 showed high permeabilities, proportional to the transmembrane pressure, and increasing with temperature (measured between room temperature and 200°C). In contrast to MFI zeolite membranes, zeogrid membrane retained selectively CO_2 from a mixture with N_2 or H_2. This is explained by the strong affinity of the hydroxylated walls of the supermicropores located in between the interposed nanoslabs. This feature could make these membranes useful for CO_2 capturing.

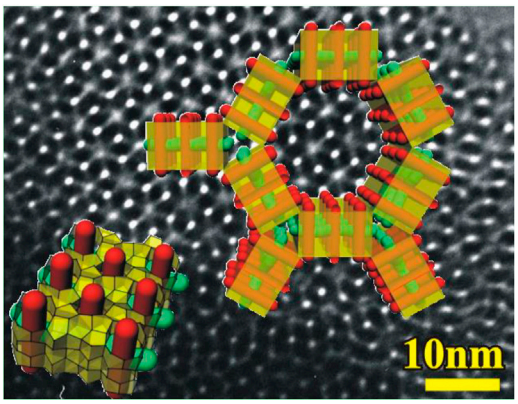

FIGURE 3 | Tiling patterns of nanoslabs in zeotile-1 superimposed on a transmission electron microscopic (TEM) image (adapted with permission from Martens et al., 2011).

Contrary to these permanent gas separations where the supermicroporosity of the zeogrid is dominating the behavior, a clear manifestation of ultramicroporosity characteristic of zeolites was observed in the pervaporation of organic solvent/water mixtures. The zeogrid membrane showed an organophilic behavior, like an MFI zeolite membrane. The permeating stream experiences the presence of hydrophobic zeolitic micropores, which are considered to be located inside the nanoslabs composing the zeogrid. Compared with siliceous MFI zeolite membranes, zeogrid membranes showed lower separation numbers and much higher fluxes.

While Zeogrids are layered materials, three-dimensional structures called zeotiles have been obtained from nanoslab suspensions using other surfactant templates (Kremer et al., 2003; Kremer et al., 2005a; Bals et al., 2009). Zeotile-1 is precipitated from the nanoslab suspension by adding aqueous solution of CTAB. CTAB induces a hexagonal ordering of double nanoslabs leading to a regular pattern of parallel channels with hexagonal and triangular shape with free diameters of 3.5 and 1.4 nm, respectively. This tiling patterns of double nanoslabs in zeotile-1 is represented as an overlay over a TEM image in **Figure 3**. The formation of triangular pores in the presence of a surfactant favoring rounded structures is quite unique. It is a strong argument for an assembly from slabs.

Two other ordered materials of this kind, zeotile-2 and zeotile-6 were also created by the addition of CTAB powder to the nanoslab suspension (Kremer et al., 2005a; Martens et al., 2011). Zeotile-2 is synthesized at high temperatures, whereas zeotile-6 is formed at low temperature. Zeotile-2 is a material showing mesostructural similarities to MCM-48, which is a gyroid with mesopores with a diameter of ca. 2.7 nm. The removal of TPA from zeotile-2 results in a substantial amount of zeolitic micropores, as evident from N_2 physisorption. The zeolite nature of the micropores was confirmed with pulse chromatographic separation of isooctane/octane mixtures. The selective access of octane to the micropores of zeotile-2 and the exclusion of isooctane confirmed the occurrence of molecular sieving similar to MFI zeolites (Kremer et al., 2005a). Zeotile-6, also synthesized using CTAB powder, has hexagonal mesoscale ordering, but the structure of this material has, thus far, not been analyzed in more detail (Martens et al., 2011).

A highlight of the zeotile family is zeotile-4 (Kremer et al., 2003). The synthesis of zeotile-4 was inspired by the synthesis of ordered mesoporous material called SBA-15 (Zhao et al., 1998). Mesostructuring is obtained using Pluronic P123 triblock copolymer, which forms micelles having hydrophilic PEO chains outside and hydrophobic PPO chains concentrated at the core of the micelle. Zeotile-4 has a unique pore architecture with fully accessible 3D porosity. Electron tomography and postsynthesis manipulations evidenced the existence of this peculiar three-dimensional pore system. The structure is built through stapling and clicking of slab units measuring ca. 8 nm × 4 nm × 1.7 nm. The nanoslab organization around the P123 micelle creates hexagonally ordered pores of ~10 nm width, which are connected *via* ~3.5-nm-wide slits as depicted in **Figure 4** (Kremer et al., 2003; Bals et al., 2009; Pulinthanathu Sree et al., 2017). The hexagonal ordering of pores as evidenced in TEM was further substantiated *via* small-angle x-ray scattering (SAXS) pattern shown in **Figure 5**.

Zeotile-4, synthesized with P123 triblock copolymer, appears like rods in which the hexagonal channels run in the long direction (**Figure 4**) (Pulinthanathu Sree et al., 2012; Pulinthanathu Sree et al., 2017). Material belonging to the same family was formed when replacing P123 ($EO_{20}PO_{70}EO_{20}$) with P104 ($EO_{27}PO_{61}EO_{27}$). SEM images of this variant of zeotile-4 reveal a more equal growth of individual tiling in the different directions and agglomeration (**Figure 6**). Nitrogen physisorption isotherm of this variant of zeotile-4 showed perfectly parallel adsorption and desorption branches of the hysteresis loop, which indicated the presence of cylindrical pores with uniform cross section and very narrow pore size distribution (**Figure 7**), which is representative of a perfect zeotile-4 material (Pulinthanathu Sree et al., 2012). The pore size is around 10 nm. The pore volume reaches 1.7 ml/g, and the specific surface area is 1,005 m^2/g. In another modification, LiCl salt was introduced in the nanoslab suspension together with Pluronic P123. Addition of LiCl at the time of synthesis yielded nicely formed hexagonal bodies as shown in **Figure 8**.

Spherical zeotile-4 particles with diameters between 3 and 10 μm were obtained using a mixture of P123 triblock copolymer and CTAB as tiling agent. This spherical shape renders the material useful as a packing of chromatographic columns (Martens et al., 2011). *Via* another adaptation of the zeotile-4 recipe, replacing P123 triblock co-polymer with P85 ($EO_{25}PO_{40}EO_{25}$) spherical porous silica particles of sizes ~5 μm were obtained (**Figure 9**). The internal porosity and brittleness are revealed by the presence of broken particles. The material had no ordering according to XRD. It is speculated that the shorter polymer chains of P85 compared with P123 and P104 could have limited the mesoscopic ordering power. The hysteresis loop suggests the presence of less uniformly shaped pores (**Figure 10**).

The presence of microporosity inside the walls of zeotiles built from zeolitic nanoslabs has been probed with chromatographic

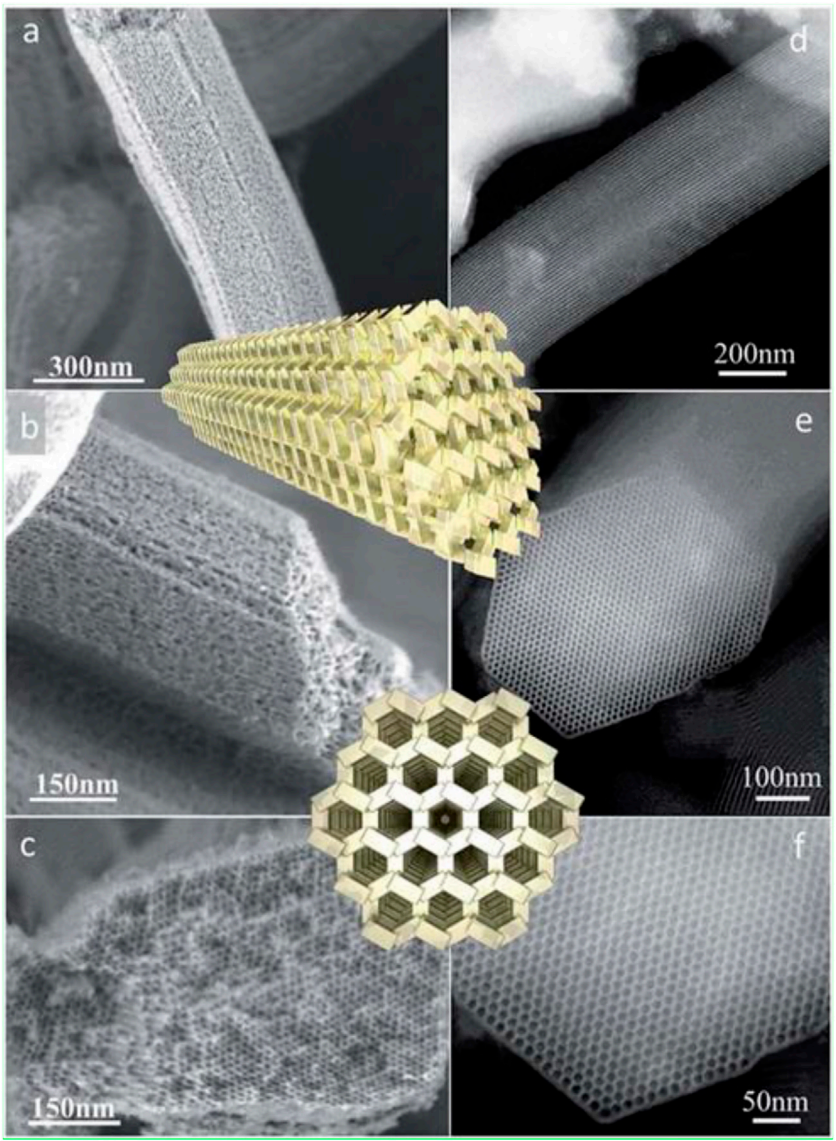

FIGURE 4 | HR-SEM images of a zeotile-4 sample: **(A,B** and b) Lateral view of slit-like and **(C)** axial view of hexagonal mesopores. HAADF-STEM images of zeotile-4 particles: **(D)** lateral view and **(E,F)** axial view with an overlay of a schematic (reproduced from Pulinthanathu Sree et al., 2017 with permission from the Royal Society of Chemistry).

separation. Preferential adsorption of n-octane in an admixture with isooctane over zeotile-2 was noted as a fingerprint of ultramicroporosity (Devriese et al., 2007). When analyzed for a broad set of molecules (*viz* C5–C9 n- and iso-alkane), zeotile-2 exhibited shape-selective discrimination between n and iso alkanes, while the MCM-48, being isostructural at mesoscale, did not show any shape selectivity. Zeotile-2 was concluded to be a hierarchical variant of MCM-48 having microporosity in its walls (Kremer et al., 2005a). Zeolitic properties were also observed in the separation of permanent gases, such as CO_2, CH_4, N_2, and H_2 (Martens et al., 2011). Zeotile-4 revealed to be an excellent HPLC (high-performance liquid chromatography) packing for the separation of oligopeptides (Martens et al., 2011).

Hierarchical silicates not only are useful for use in separation and catalytic processes, they can also serve as a template, creating a negative replica with a different composition. This approach, on the one hand, offers options, for example, to generate uniquely shaped materials consisting, e.g., of platinum, titanium dioxide and, on the other hand, also allows to investigate the pore architecture from a different perspective, probing not only the shape but also the accessibility. Zeotiles, and especially zeotile-4 with its unique pore architecture (**Figure 4**), are an attractive candidate to serve as a hard template for replication. The 3-dimensional channel system of zeotile-4 was replicated with platinum *via* atomic layer deposition (ALD) (Pulinthanathu Sree et al., 2017). The ALD process involved alternating pulses

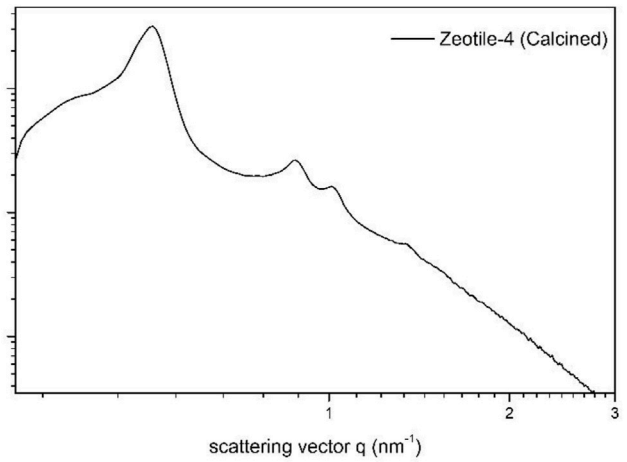

FIGURE 5 | Small-angle x-ray scattering pattern of calcined zeotile-4 (reproduced from Pulinthanathu Sree et al., 2012 with permission from the American Chemical Society).

of (methylcyclopentadienyl) trimethylplatinum (MeCpPtMe3) vapor and O_3 gas at 200°C. The replica was liberated by selective digestion of the zeotile using HF. The replica shown in **Figure 11** is micrometers long, fully connected free-standing Pt nanostructures replicating the pores of the zeotile-4. High-resolution electron microscopy (SEM, STEM, and TEM) combined with electron tomography evidenced the presence of hexagonal Pt nanorods of ~11 nm, which are replications of the main channels of zeotile-4. The replica confirms the hexagonal shape of the channels, with sharp corners, confirming in this way that the zeolite is built from slabs like a house of cards. Interestingly, in the replica, the hexagonal rods stay firmly connected and fixed in a hexagonal pattern (**Figure 12**). This fixation is interpreted by the presence of small linkages, which can be platinum features obtained from replication of the slit-like connecting pores. The Pt replica was found to have exceptional properties as an electrocatalyst for the hydrogen evolution reaction of water splitting and also as high-surface area microelectrode for biomedical sensing. The low impedance and high charge injection capacity could find applications in neural stimulation implants.

Using ALD, zeotile-4 could be filled with TiO_2 as well (Pulinthanathu Sree et al., 2012). By varying the exposure times of the zeotile-4 material to Ti precursor, the penetration depth into the main channel and the slit-like channels could be varied. Zeotile-4 particles partially filled with TiO_2 in their rim with remaining porosity in the interior could be interesting for applications, such as photocatalysis.

For applications such as photocatalysis, thin films are desirable. Flexible and highly porous thin films without particular ordering have been prepared by spin coating nanoslab suspensions with P123 triblock copolymer meant for preparing zeotile-4 (Sree et al., 2011). By slight adjustments in the synthesis parameters, thin films with porosities ranging from 70 to 90% and varying pore sizes of 6–18 nm were obtained. These extremely porous thin films turned out to be surprisingly robust as well as flexible as evidenced with ellipsometric porosimetry. The films exhibit reversible shrinkage up to 30% by capillary condensation of toluene adsorbate. Using ALD, the porosity was systematically filled according to the number of ALD cycles (**Figure 13**). These ALD TiO_2 layers can be transformed thermally to uniformly disperse anatase nanoparticles (sizes ~4 nm) spread inside the mesopores of these thin films. These photocatalytic films showed excellent photocatalytic activity in methylene blue degradation (Sree et al., 2013) (**Figure 13**).

The potential of these films as part of a cheap, portable, and integrated breath ammonia-sensing instrument was investigated (Yebo et al., 2012). Silicon photonic microring resonators coated with this mesoporous silica, and further functionalized with Al-ALD to introduce acid sites, were found to be effective for ammonia sensing. Microring resonator sensors with these films showed fast and reversible response to ammonia with good selectivity relative to CO_2.

Zeotile-1 and zeogrids have been used as support for photoluminescent europium and terbium. Discrete types of luminescence were observed, in contrast to zeolites in which a heterogenous distribution of luminescences were observed (Tiseanu et al., 2006; Tiseanu et al., 2008c; Tiseanu et al., 2008a; Tiseanu et al., 2008b; Tiseanu et al., 2009).

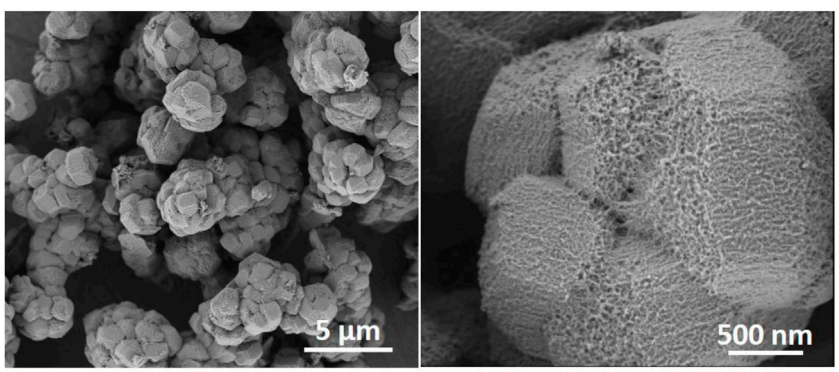

FIGURE 6 | HR-SEM images of zeotile-4synthesized using Pluronic P104 as mesostructuring agent, material from the same family that is discussed in Pulinthanathu Sree et al. (2012) and Pulinthanathu Sree et al. (2017).

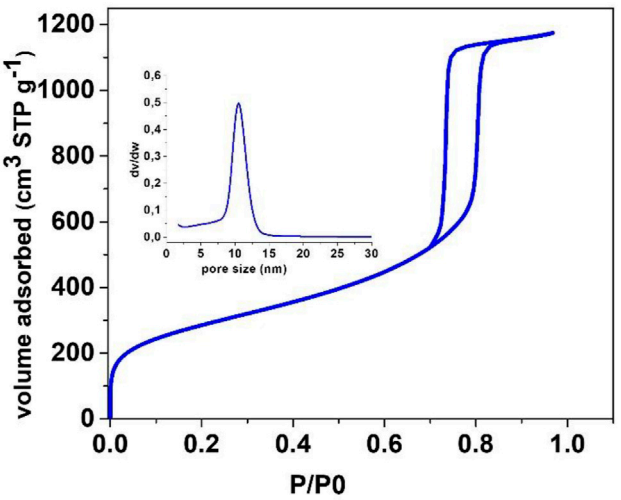

FIGURE 7 | N_2 physisorption isotherm of calcined zeotile-4 made using Pluronic P104, similar class of material discussed in Pulinthanathu Sree et al. (2012) and Pulinthanathu Sree et al. (2017). The pore size distribution PSD is shown in the inset.

The potential of zeogrid and zeotiles in catalysis has been evaluated in hydroisomerization and hydrocracking, catalytic cracking, alkylation, and epoxidation reactions. The detailed reaction product distribution from hydroisomerization and hydrocracking of model n-alkanes, such as n-decane, gives detailed insight in the pore architecture of a microporous material (Martens et al., 1984; Martens and Jacobs, 1986; Souverijns et al., 1994). The test is applicable when the material has BrØnsted acidity. A trace amount of platinum is needed to provide alkene hydrogenation and alkane dehydrogenation activity. The porosity of zeogrids with aluminosilicate composition was probed with the n-decane test (Aerts et al., 2003, 2004). The common property of zeogrids built from nanoslabs (**Figure 2**) is the exposure of faces with openings made from intersected crossings of zigzag channels with straight channels. The same framework termination is present in the walls of the supermicropores. Molecular models revealed these pockets to be much wider than the channel segments being confined by 10 rings. Due to this peculiar framework termination, a zeogrid does not show molecular shape selectivity similar to MFI zeolites and nanosheets developed in other crystallographic directions (Verheyen et al., 2013). In this respect, the zeogrids resemble MCM-22 zeolite, in which surface pockets are also responsible for the catalytic activity (Aerts et al., 2003, Aerts et al., 2004) The isomerization yield from zeogrids and the nanozeolite assembled from nanoslabs was up to 70%, which is among the highest values reached with zeolites (Martens et al., 1991). In n-decane conversion, a freshly assembled MFI zeolite assembled from nanoslabs and a zeogrid show similar selectivities. Only after changing the particle morphology and elimination of the supermicroporosity upon ripening of the crystals in the synthesis medium can shape selectivity typical of ZSM-5 be manifested. Skeletal isomerization of long alkanes on 10-ring zeolites is a case of pore mouth catalysis (Martens et al., 1995, Martens et al., 2001; Claude and Martens, 2000). The framework termination mode appears to be critical for obtaining molecular shape selectivity (Aerts et al., 2004).

Zeotile-4 has been provided with BrØnsted acid sites using atomic layer deposition (ALD) aluminum in repeated cycles of trimethylaluminum deposition and hydrolysis. The catalytic behavior of modified zeotile-4 in hydrocracking and hydroisomerization was similar to an ultrastable Y zeolite also having a combination of micropores and mesopores (Detavernier et al., 2011). Catalytic cracking of isooctane and methyl cyclohexane was performed over zeogrid and compared with ultrastable Y and ZSM-5 zeolites (Borm et al., 2010; Van Borm et al., 2010). Zeogrid exhibits a product distribution similar to that obtained on a ultrastable Y zeolite, e.g., a high selectivity to C_4 products as well as a relatively high selectivity toward branched products. Here again, like in the n-decane test, the active sites of zeogrid are situated in the surface pockets of supermicropores and external surfaces imposing little steric constraint.

Diisopropylation of naphthalene to 2,6-diisopropylnaphthalene (2,6-DIPN) is an intermediate step of the synthesis of 2,6-naphthalene dicarboxylic acid. Typical naphthalene diisopropylation catalysts are ultrastable Y and mordenite zeolites (Bouvier et al., 2010). Zeogrids were found to be equally active than the reference catalysts but produced significantly more diisopropylated (DIPN) and polyisopropylated (PIPN) products,

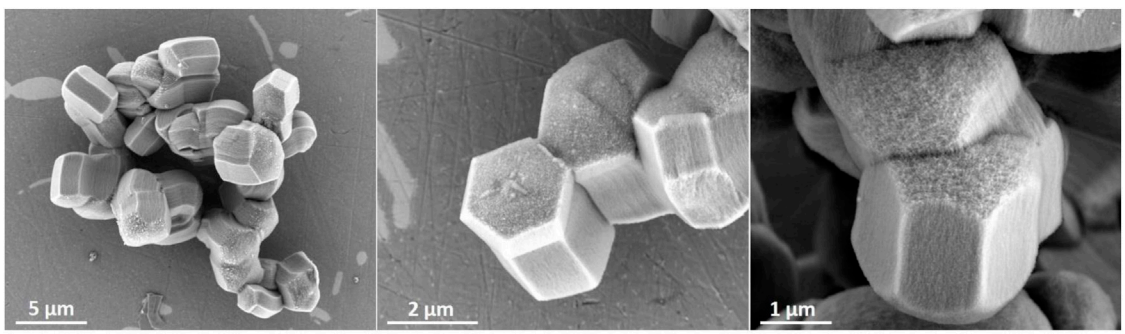

FIGURE 8 | Zeotile-4 synthesized using the procedure discussed in Pulinthanathu Sree et al. (2012) and Pulinthanathu Sree et al. (2017) with the addition of LiCl to Pluronic P123.

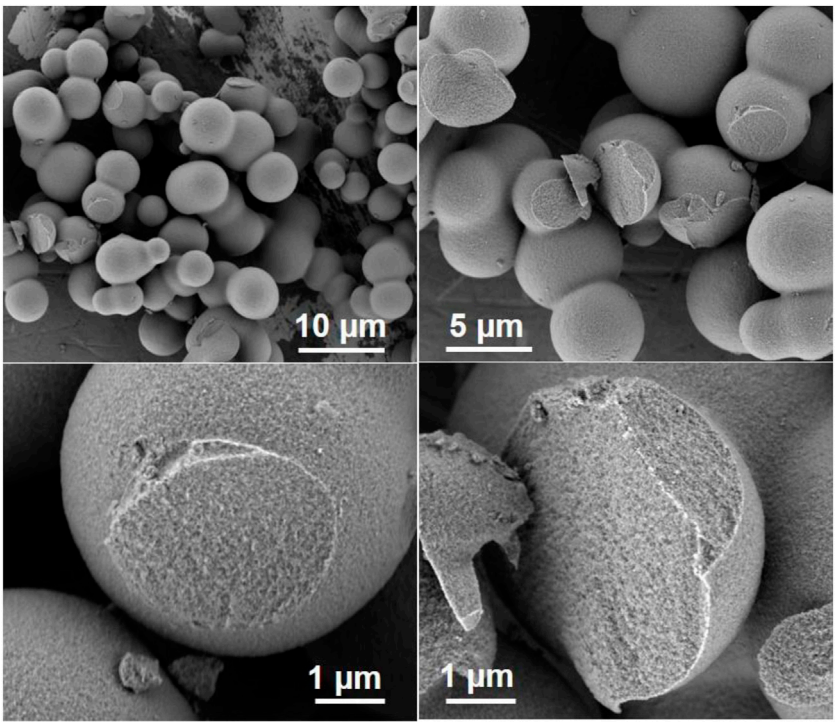

FIGURE 9 | Spherical silica similar to those obtained from Martens et al. (2011) *via* modified recipe of zeotile-4 using P85.

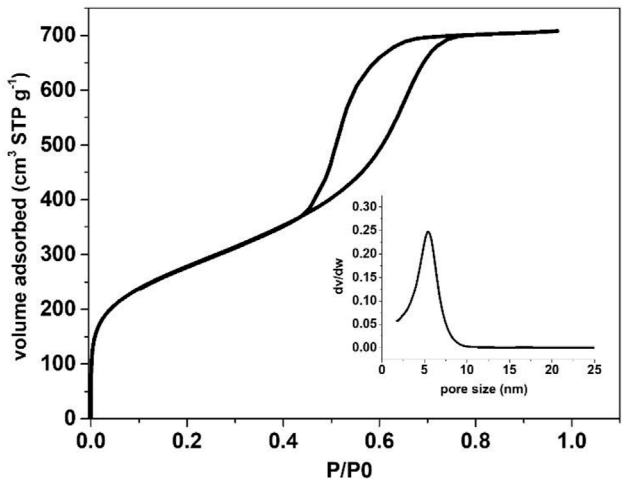

FIGURE 10 | N2 physisorption isotherm of spherical silica particles created *via* adapted recipe of zeotile-4 from Martens et al. (2011) and Pulinthanathu Sree et al. (2012) using Pluronic P85 copolymer.

and specifically the desired 2,6-DIPN. This property was ascribed to catalytic turnovers in supermicropores and their surface pockets being wide enough for the desired diisopropylation but limiting the over-alkylation by steric constraints (Martens et al., 2011). Zeogrid and zeotiles (zeotile-2, −4, −6) doped with Ti exhibit excellent catalytic activity and selectivity in cyclohexane epoxidation using tert-butylhydroperoxide (TBHP) (Reichinger et al., 2010). Depending on the organic solvent, the performance was even better than benchmark catalysts Ti-MCM-41 and TS-1 (Khouw et al., 1994; Srinivas et al., 2004).

Hierarchical COK-X ordered mesoporous materials

SBA-15 is an exponent of the ordered mesoporous silicate materials appreciated for its uniform porosity and excellent hydrothermal stability. An inconvenient aspect of the synthesis of SBA-15 is its synthesis in concentrated hydrochloric acid causing corrosion problems to the equipment and lots of chemical waste. This motivated the quest for alternatives synthesized under more gentle conditions (Kim et al., 2000; Kim et al., 2001), and COK-12 is one of these materials (Jammaer et al., 2009). COK-12 is a highly 2D ordered mesoporous structure with uniform mesopores at mesoscale similar to SBA-15. It is synthesized at room temperature using a cheap silicon source (waterglass) and quasi-neutral pH established in the synthesis mixture by using citric acid/citrate buffer (Jammaer et al., 2009). The synthesis procedure offers much flexibility in further tuning of the mesopore width by increasing the temperature and varying the pH. In the optimized procedure, an aqueous solution of Pluronic P123 triblock copolymer is prepared to which citric acid and trisodium citrate are added to obtain a pH buffer. Subsequently, sodium silicate solution is added. The formation of COK-12 occurs spontaneously at room temperature. COK-12 particles have a hexagonal disc-like morphology as observed with

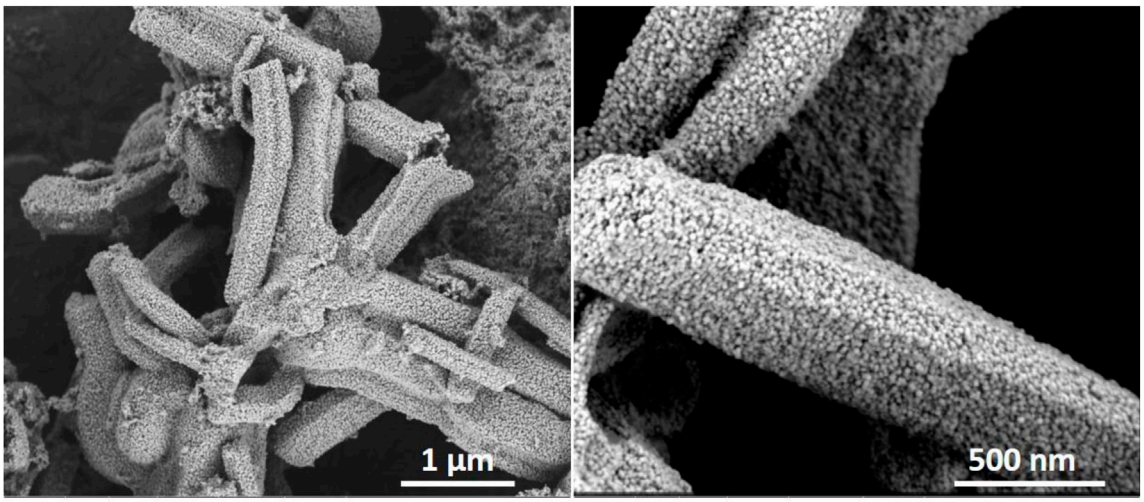

FIGURE 11 | Free-standing Pt replicas of zeotile-4 obtained after silica digestion of zeotile-4 using HF, material discussed in Pulinthanathu Sree et al. (2017).

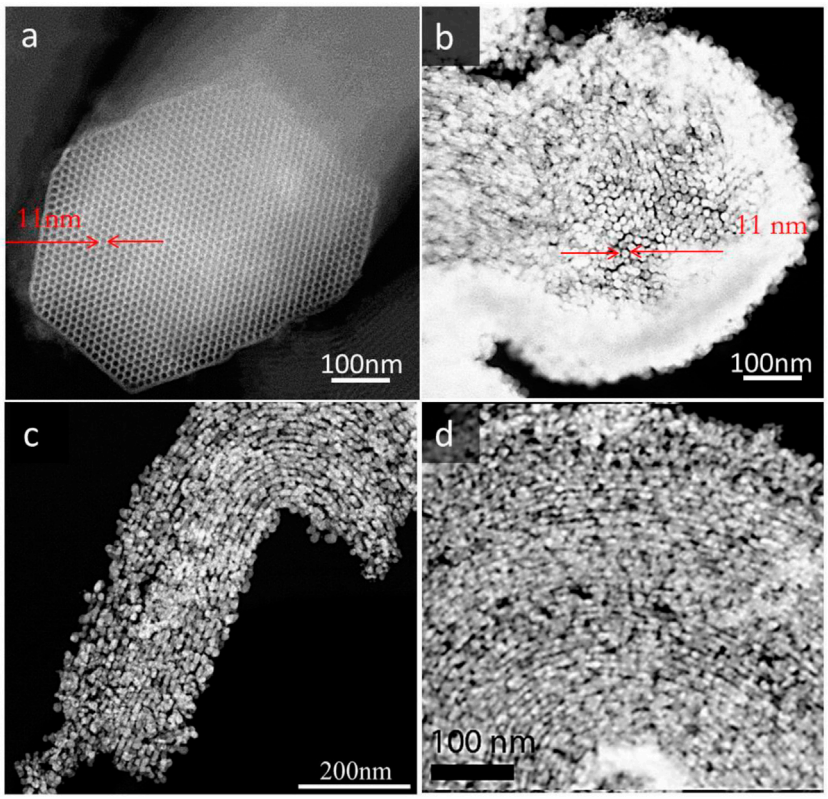

FIGURE 12 | HAADF-STEM image of the parent zeotile-4 **(A)** and that of its platinum replica **(B)** along the cross section showing the hexagonal rods being exact replications of the main channels with platinum. Lateral views of the replica **(C,D)** showing the small struts of Pt lining up with the main rods being replicas of the interconnecting narrow pores (reproduced from Pulinthanathu Sree et al., 2017 with permission from the Royal Society of Chemistry).

HRSEM (**Figure 14**). This platelet morphology is very attractive given the shortness of the mesopores, limiting the path length for molecular diffusion.

This simple synthesis procedure can be used in a continuous manufacturing scheme (Jammaer et al., 2011). A stream of citric acid-/sodium citrate-buffered solution of

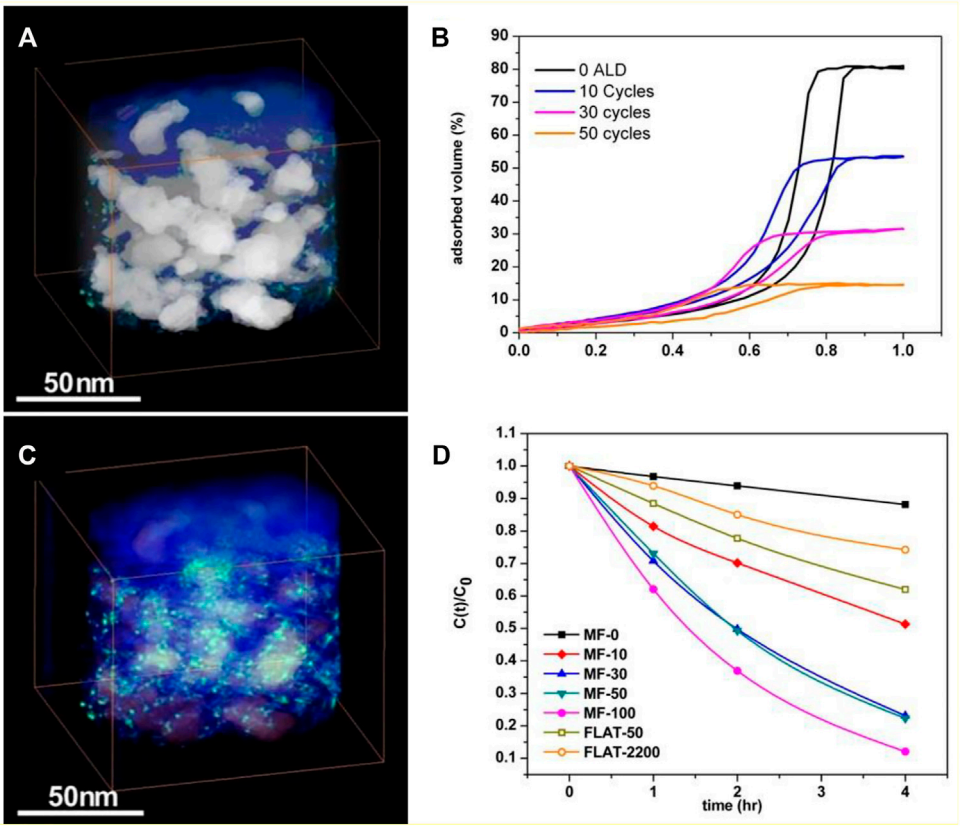

FIGURE 13 | Electron tomography reconstructions of the atomic layer deposition (ALD) deposited TiO_2 (50 cycles) containing mesoporous silica film made of nanoslabs having 80% porosity **(A,C)**: 3D voltex visualization of the reconstruction of a part of the film; mesopores highlighted in white in **(A)**, and anatase particles in green in **(C)**. Toluene adsorption isotherms **(B)** determined using EP on different pieces of the same film after the indicated ALD treatments. **(D)** Photocatalytic degradation of methylene blue on the TiO_2-loaded films (MF-x), with x referring to the number of ALD cycles; FLAT-x denotes a silicon wafer coated with TiO_2 using x ALD cycles (reproduced from Sree et al., 2011, Sree et al., 2013 with permission from the Royal Society of Chemistry).

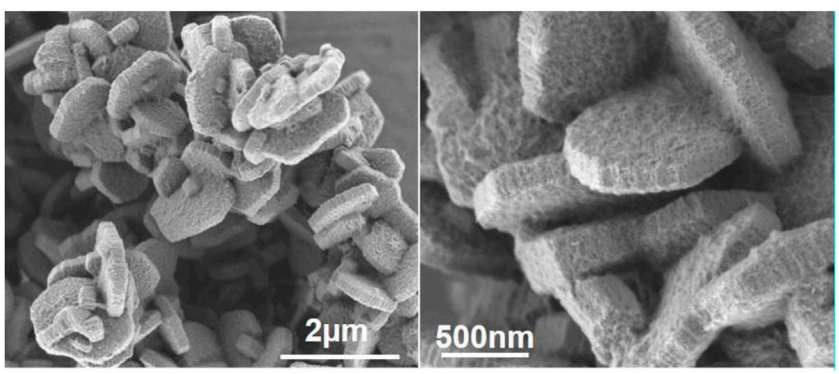

FIGURE 14 | HR-SEM images revealing the hexagonal platelet morphology of COK-12.

Pluronic P123 polymer is combined with a stream of diluted sodium silicate. The formation of COK-12 is almost instantaneous such that a suspension of COK-12 can be recovered at the outlet of a conduct in which the mixing of the two streams occurs.

An attractive feature of the COK-12 synthesis is that the assembly process can be interrupted at any intermediate stage by limiting the amount of sodium silicate added. The synthesis mechanism revealed by SAXS (small-angle x-ray scattering) using this experimental procedure is represented in **Figure 15**. In the

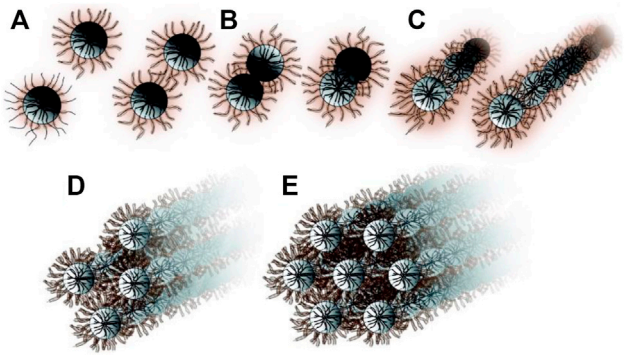

FIGURE 15 | Formation mechanism of COK-12. **(A)** Core–shell P123-silica micelle formation by incorporation of silicate oligomers in the layer of PEO chains extending toward the solution, **(B)** loss of steric stabilization at a critical point of silica addition, **(C)** spherical micelles aggregate to form cylindrical features, **(D,E)** agglomeration of cylinders eventually to hexagonally ordered structure upon final addition of silica (reprinted with permission from Jammaer et al., 2011, Copyright 2011 American Chemical Society).

first step, spherical core–shell P123-silica micelles are formed. Silicate oligomers are accumulating selectively in the polar PEO shell of the triblock micelles. The steric stabilization of these micelles will be lost at critical point of silica addition. This destabilization of the emulsion leads to aggregation of the spherical core-shell PPO–silica + PEO particles to cylindrical features. Upon further addition of silicate, these elongated assemblies align and coalesce eventually shaping the final hexagonal platelets. This mechanism explains why the mesopores cross the platelets. The neutral pH minimizing the charge on the silicate oligomers promoting their accumulation in the PEO rim of the uncharged P123 micelle is at the origin of this unique formation mechanism. High-resolution TEM reveals the undulated nature of the mesopores, which originates from the linear assemblies of spherical P123 micelles (Jammaer et al., 2009).

The ease of preparation and the unique morphology with uniform, short-ordered mesopores with diameters tunable in the range from 5 to 10 nm prompted researchers to consider using COK-12 for multiple purposes. Ordered mesoporous materials, when used as support for poorly soluble drugs, enhance the bioavailability (Mellaerts et al., 2007; Vialpando et al., 2011b). In absence of water, the drug molecules show high affinity for the mesopore walls and spread along the internal surfaces of the mesopores. The hydrophilic/hydrophobic balance is such that upon contacting the drug-loaded support with aqueous solution, water wins the adsorption competition such that the drug molecules are expulsed from the pores generating this way a supersaturated solution. In oral drug formulations, the gastrointestinal track provides the water for such competition effect. The generation of a supersaturated drug solution leads to enhanced bioavailability. The phenomenon has been observed in the early studies with the antimycotic itraconazole in SBA-15, zeotile-4, and COK-12 and later with many more poorly soluble active compounds (Mellaerts et al., 2007; Speybroeck et al., 2009; Vialpando et al., 2011b). The bioavailability-enhancing effect of ordered mesoporous silica has been confirmed first *in vitro*, and later in animal studies (Bukara et al., 2016a), and finally in man in a phase I clinical study using fenofibrate as a model molecule (Bukara et al., 2016b). COK-12 also appeared to be advantageous for tableting. Because of its slightly thicker walls and higher condensation degree of the silicate framework due to the higher synthesis pH compared with SBA-15, COK-12 is more resistant to compaction (Vialpando et al., 2011a). Hydrophobic molecules can even be incorporated already during COK-12 synthesis itself because of their affinity to the PPO moiety of the triblock copolymer. Molecules like flurbiprofen have been incorporated in the cores of P123 micelles. Given the mild conditions of COK-12 synthesis (room temperature, quasi neutral pH), the molecules are encapsulated together with the triblock copolymer without deterioration. Silica capsules enclose P123 triblock copolymer micelles for flurbiprofen storage and release (Kerkhofs et al., 2015a).

In the application field of waste water purification, COK-12 was grafted with graphene oxide (GO) and evaluated for adsorption of methylene blue (Henning et al., 2019). The GO-grafted COK-12 was found to have superior adsorption capacity in comparison with other GO-grafted ordered mesoporous materials. GO grafting also had a positive influence on the stability of COK-12, even up to pH 10. In another study, Co_3O_4/COK-12 showed fast effective adsorption of methylene blue, thus, qualifying it as a low-cost material for elimination of methylene blue dye from wastewater (Jyothi et al., 2017).

COK-12 has also been investigated for photocatalytic applications. Anatase TiO_2 nanoparticles, especially in size ranges of ~10 nm and smaller, have excellent photocatalytic activity, but their use entails toxicity and environmental risks. Immobilization of these nanoparticles on to porous solid matrices is a way to overcome this problem. COK-12 is an effective support for anatase nanoparticles. Here again, the platelet morphology is favorable for the preparation of the photocatalyst merely by impregnation of titanium(iv) isopropoxide followed by calcination (Wee et al., 2016). In the photocatalytic degradation of various organic pollutants like 1-adamantanol, rhodamine 6G, and methylene blue under UV light irradiation, anatase-loaded COK-12 photocatalyst exhibited enhanced activity than the commercially available TiO_2 catalyst. Similar advantages of COK-12 over other ordered mesoporous materials were encountered when confining hematite iron oxide (α-Fe_2O_3) nanoparticles for visible light photocatalysis (Wee et al., 2015). The structural details and distribution of these nanorods in the COK-12 channels can be appreciated in HAADF-STEM images and three-dimensional visualization by electron tomography in **Figure 16**.

The ease of synthesis, disc-like morphology, homogenous particle size, and short mesopores of COK-12 make it attractive as a filler of mixed matrix membranes (MMMs) for gas separations (Khan et al., 2015). Also, in the field of heterogeneous catalysis, some gains have been achieved by using COK-12 as support. For instance, COK-12-supported Co_3O_4 was found to be an excellent catalyst for oxidative ethylbenzene dehydrogenation to styrene (Pochamoni et al., 2015). In another report, MoO_3/COK-12 catalyst with 14 wt%

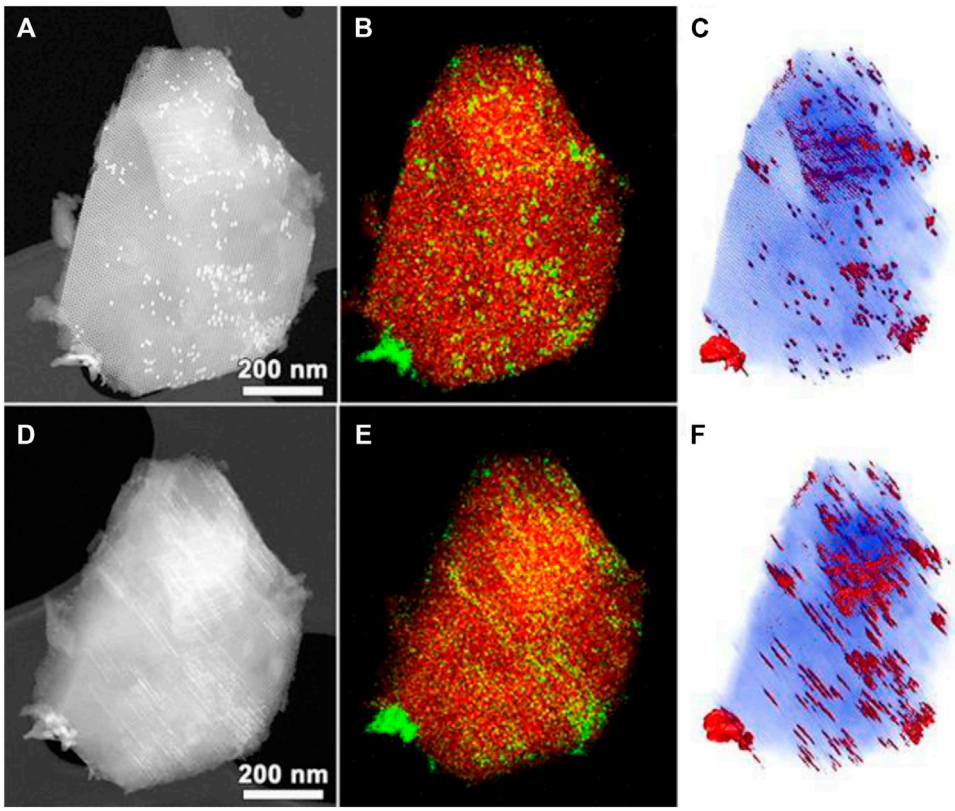

FIGURE 16 | Electron microscopic investigation of α-Fe_2O_3@COK-12. **(A–C)** HAADF-STEM image of α-Fe2O3@COK-12, EDX elemental mapping (green—Fe and red—Si), HAADF-STEM tomography reconstruction, respectively, along the pore direction and **(D–F)** similar observations along the direction slightly perpendicular to the pore (reproduced from Wee et al., 2015 with permission from the Royal Society of Chemistry).

MoO_3 loading was found to be very active in this reaction as well (Pochamoni et al., 2014). Na_2WO_4–Mn/SiO_2 COK-12 catalyst was conceived as a catalyst for oxidative coupling of methane. COK-12 was found to be convenient for catalyst formulations like granules and monoliths (Colmenares et al., 2018).

COK-19 is another ordered mesoporous silica material having cubic symmetry, which is created at similar mild synthesis conditions as for COK-12, but using Pluronic F127 triblock co-polymer (EO100 PO70 EO100) instead of P123 (Kerkhofs et al., 2015b). Alike COK-12, COK-19 is also formed instantaneously when the buffered P127 solution is brought in contact with sodium silicate solution. The material has isolated spherical mesopores with diameters of ca. 7 nm separated *via* thick pore walls provided with interconnecting micropores. Enhancing the synthesis temperature to 50°C and 70°C caused widening of the main cavities as well as the interconnecting pores according to electron tomography. This enlargement can be explained by the swelling of the Pluronic micelles acting as mesoscopic templates for the porosity. HR SEM images unveiled the morphology of COK-19 to be that of collectively grown truncated octahedrons (**Figure 17**). Progressive addition of the silica in steps causes interruption of the formation process, which proceeds stepwise like in the case of COK-12 (**Figure 15**).

Hierarchical COK-X metal–organic frameworks

The generation of hierarchical MOF materials with permanent mesoporosity next to microporosity is not straightforward. The use of secondary building units and surfactant-templated synthesis have been explored. Many synthesis attempts result in irregular mesopores that collapse after surfactant removal (Qiu et al., 2008; Sun et al., 2011). The overview of zeotiles and ordered mesoporous materials in the previous sections revealed how pore hierarchy can be obtained using a dual-template approach, with a molecular template for micropores, such as TPA for making nanoslabs, and micellar templates for shaping mesopores, which typically are surfactant micelles. A same dual-template approach can be followed to create hierarchical metal–organic frameworks (MOFs). The first MOF for which this approach has been successful was a copper benzene-1,3,5-tricarboxylate HKUST-1, $Cu_3(BTC)_2$ (Chui et al., 1999). It is a microporous MOF with small octahedral cages connected to form two types of large cavities. One of these large cages is ideally suited for encapsulation of polyoxometalates (POMs). Strong interaction between Cu(II) and Keggin type HPW ions leads to spontaneous, room temperature self-assembly of a microporous HKUST-1 HPW@$Cu_3(BTC)_2$ coined COK-16 (Bajpe et al., 2010, Bajpe et al., 2011). The assembly of the MOF proceeds by initial

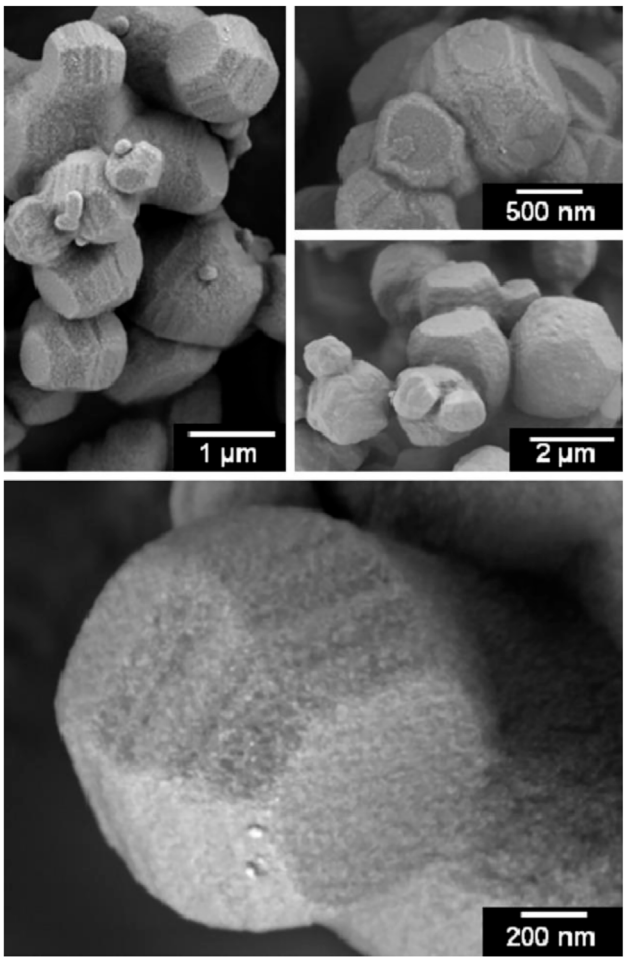

FIGURE 17 | HRSEM images of COK-19 (reprinted with permission from Kerkhofs et al., 2015b, Copyright 2015 American Chemical Society).

formation of POM-encapsulating cages, which connect in space to for the microporous MOF. Encapsulation of the POM not only enables room temperature synthesis of $Cu_3(BTC)_2$ MOF but also protects the structure against degradation in heated, humid conditions (Mustafa et al., 2011) and provides it with cation exchange properties (Bajpe et al., 2013), enabling its conversion into a photoluminescent material by incorporation of rare earth ions and exploiting the metal–organic framework as sensitizer (Mustafa et al., 2014).

By adding cetyltrimethylammonium bromide (CTAB) to the synthesis as secondary structure-directing agent, it was discovered that the aggregation sequence of the elemental cages could be altered. A robust hierarchical MOF material, COK-15, schematically shown in **Figure 18**, with strictly repetitive 5-nm-wide mesopores was obtained from which the CTAB could be removed without structural collapse (Wee et al., 2012). The robustness of this particular MOF originates from the reinforcement of the mesopore walls with Keggin POMs filling systematically one of the cages of the HKUST-1 structure composing the walls.

The copper benzene-1,3,5-tricarboxylate composition is particularly versatile for creating hierarchical materials.

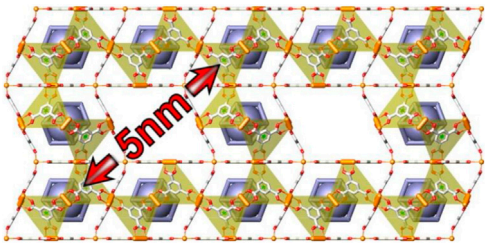

FIGURE 18 | Schematic representation of hierarchical metal–organic framework (MOF), COK-15 (reprinted with permission from Wee et al., 2012, Copyright 2012 American Chemical Society).

Departing from a dense $Cu_3(BTC)_2$ phase with excess copper, thermal expansion created a sequence of new materials with mesoporosity increasing in dimensionality to reach a three-dimensional interconnected hierarchical pore system in an MOF-coined COK-18 (Wee et al., 2017). The volumetric expansion is assisted by the systematic presence of Cu(II) unsaturated coordination sites. COK-18, by its special chemistry of its pore walls, exhibits peculiar adsorption enthalpies and entropies in hydrocarbon separation.

Hierarchical-layered double hydroxides

A dual template approach has been applied to fabricate layered double hydroxides (LDH) with the shape of nanotubes (Morais et al., 2017). In this synthesis procedure, hydrolysis of Zn^{2+}, Al^{3+}, and Eu^{3+}cations was performed in the presence of 1,3,5-benzenetricarboxylate anion-shaping primary units, while non-ionic worm-like micelles were used to arrange the oligo layering at longer length scales into easily accessible cylindrical mesopores. When provided with CdTe quantum dots, enhanced overall luminescence behavior was obtained.

CONCLUSION

Hierarchical materials with structural order and porosity at different levels, and especially the combination of micropores and mesopores, are very useful in catalysis, adsorptive separation, hosting of functional nanoparticles, and controlled release for a myriad of applications. For all these applications, the stability of the material after evacuation of the molecular and supramolecular templates from the pores is a primordial property. In the world of silicates, the paradigm of creating building units such as zeolitic nanoslabs and assembling them in grids and tiles in two- and three-dimensional space has been very successful. Zeogirds and zeotiles and materials like spacious films have demonstrated their usability. In MOF materials, the use of templates is less obvious given the structure-directing action at the ligation of the metal centers by themselves. Nevertheless, MOFs are fragile materials, and by permanently reinforcing the cages with an inorganic primary template, such as with Keggin POM in HKUST1, the dual-template approach was met with success. The dual-

template approach is quite generic and has been used to synthesize hierarchical LDH materials as well.

AUTHOR CONTRIBUTIONS

All authors listed have made a substantial, direct, and intellectual contribution to the work and approved it for publication.

ACKNOWLEDGMENTS

The authors acknowledge the Flemish Government for the long-term structural funding (Methusalem), for financial support as International Research Infrastructure (I001321N: Nuclear Magnetic Resonance Spectroscopy Platform for Molecular Water Research) and the European Union's Horizon 2020 research and innovation program under grant agreement No. 834134 (WATUSO).

REFERENCES

Aerts, A., Follens, L. R. A., Haouas, M., Caremans, T. P., Delsuc, M.-A., Loppinet, B., et al. (2007). Combined NMR, SAXS, and DLS Study of Concentrated Clear Solutions Used in Silicalite-1 Zeolite Synthesis. *Chem. Mater.* 19, 3448–3454. doi:10.1021/cm070693j

Aerts, A., Huybrechts, W., Kremer, S. P. B., Kirschhock, C. E. A., Theunissen, E., Isacker, A. V., et al. (20031888). n-Alkane Hydroconversion on Zeogrid and Colloidal ZSM-5 Assembled from Aluminosilicate Nanoslabs of MFI Framework Type. *Chem. Commun.*, 1888. doi:10.1039/b304624a

Aerts, A., van Isacker, A., Huybrechts, W., Kremer, S. P. B., Kirschhock, C. E. A., Collignon, F., et al. (2004). Erratum to "Decane Hydroconversion on Bifunctional Zeogrid and Nano-Zeolite Assembled from Aluminosilicate Nanoslabs of MFI Framework Type" [Appl. Catal. A: General 257 (2004) 7-17]. *Appl. Catal. A: Gen.* 267, 273. doi:10.1016/j.apcata.2004.02.029

Bajpe, S. R., Breynaert, E., Martin-Calvo, A., Mustafa, D., Calero, S., Kirschhock, C. E. A., et al. (2013). COK-16: A Cation-Exchanging Metal–Organic Framework Hybrid. *Chempluschem* 78, 402–406. doi:10.1002/cplu.201300080

Bajpe, S. R., Breynaert, E., Mustafa, D., Jobbágy, M., Maes, A., Martens, J. A., et al. (2011). Effect of Keggin Polyoxometalate on Cu(ii) Speciation and its Role in the Assembly of Cu3(BTC)2 Metal–Organic Framework. *J. Mater. Chem.* 21, 9768. doi:10.1039/c1jm10947b

Bajpe, S. R., Kirschhock, C. E. A., Aerts, A., Breynaert, E., Absillis, G., Parac-Vogt, T. N., et al. (2010). Direct Observation of Molecular-Level Template Action Leading to Self-Assembly of a Porous Framework. *Chem. Eur. J.* 16, 3926–3932. doi:10.1002/chem.200903239

Bals, S., Batenburg, K. J., Liang, D., Lebedev, O., Van Tendeloo, G., Aerts, A., et al. (2009). Quantitative Three-Dimensional Modeling of Zeotile through Discrete Electron Tomography. *J. Am. Chem. Soc.* 131, 4769–4773. doi:10.1021/ja8089125

Borm, R. V., Reyniers, M.-F., Martens, J. A., and Marin, G. B. (2010). Catalytic Cracking of Methylcyclohexane on FAU, MFI, and Bimodal Porous Materials: Influence of Acid Properties and Pore Topology. *Ind. Eng. Chem. Res.* 49, 10486–10495. doi:10.1021/ie100429u

Bouvier, C., Buijs, W., Gascon, J., Kapteijn, F., Gagea, B. C., Jacobs, P. A., et al. (2010). Shape-selective Diisopropylation of Naphthalene in H-Mordenite: Myth or Reality? *J. Catal.* 270, 60–66. doi:10.1016/j.jcat.2009.12.005

Bukara, K., Schueller, L., Rosier, J., Daems, T., Verheyden, L., Eelen, S., et al. (2016a). *In Vivo* Performance of Fenofibrate Formulated with Ordered Mesoporous Silica versus 2-Marketed Formulations: A Comparative Bioavailability Study in Beagle Dogs. *J. Pharm. Sci.* 105, 2381–2385. doi:10.1016/j.xphs.2016.05.019

Bukara, K., Schueller, L., Rosier, J., Martens, M. A., Daems, T., Verheyden, L., et al. (2016b). Ordered Mesoporous Silica to Enhance the Bioavailability of Poorly Water-Soluble Drugs: Proof of Concept in Man. *Eur. J. Pharmaceutics Biopharmaceutics* 108, 220–225. doi:10.1016/j.ejpb.2016.08.020

Burkett, S. L., and Davis, M. E. (1995). Mechanisms of Structure Direction in the Synthesis of Pure-Silica Zeolites. 1. Synthesis of TPA/Si-ZSM-5. *Chem. Mater.* 7, 920–928. doi:10.1021/cm00053a017

Chui, S. S.-Y., Lo, S. M.-F., Charmant, J. P. H., Orpen, A. G., and Williams, I. D. (1999). A Chemically Functionalizable Nanoporous Material [Cu 3 (TMA) 2 (H 2 O) 3] N. *Science* 283, 1148–1150. doi:10.1126/science.283.5405.1148

Claude, M. C., and Martens, J. A. (2000). Monomethyl-Branching of Long N-Alkanes in the Range from Decane to Tetracosane on Pt/H-ZSM-22 Bifunctional Catalyst. *J. Catal.* 190, 39–48. doi:10.1006/jcat.1999.2714

Colmenares, M. G., Simon, U., Cruz, O., Thomas, A., Goerke, O., and Gurlo, A. (2018). Batch and Continuous Synthesis Upscaling of Powder and Monolithic Ordered Mesoporous Silica COK-12. *Microporous Mesoporous Mater.* 256, 102–110. doi:10.1016/j.micromeso.2017.08.002

Davis, T. M., Drews, T. O., Ramanan, H., He, C., Dong, J., Schnablegger, H., et al. (2006). Mechanistic Principles of Nanoparticle Evolution to Zeolite Crystals. *Nat. Mater* 5, 400–408. doi:10.1038/nmat1636

Detavernier, C., Dendooven, J., Pulinthanathu Sree, S., Ludwig, K. F., and Martens, J. A. (2011). Tailoring Nanoporous Materials by Atomic Layer Deposition. *Chem. Soc. Rev.* 40, 5242. doi:10.1039/c1cs15091j

Devriese, L. I., Cools, L., Aerts, A., Martens, J. A., Baron, G. V., and Denayer, J. F. M. (2007). Shape Selectivity in Adsorption Ofn- and Iso-Alkanes on a Zeotile-2 Microporous/Mesoporous Hybrid and Mesoporous MCM-48. *Adv. Funct. Mater.* 17, 3911–3917. doi:10.1002/adfm.200700008

Dokter, W. H., van Garderen, H. F., Beelen, T. P. M., van Santen, R. A., and Bras, W. (1995). Homogene und heterogene Kristallkeimbildung bei Zeolithen. *Angew. Chem.* 107, 122–125. doi:10.1002/ange.19951070133

Dubinin, M. M. (1968). Porous Structure of Adsorbents and Catalysts. *Adv. Colloid Interf. Sci.* 2, 217–235. doi:10.1016/0001-8686(68)85004-3

Flanigen, E. M., Bennett, J. M., Grose, R. W., Cohen, J. P., Patton, R. L., Kirchner, R. M., et al. (1978). Silicalite, a New Hydrophobic Crystalline Silica Molecular Sieve. *Nature* 271, 512–516. doi:10.1038/271512a0

Haouas, M., Petry, D. P., Anderson, M. W., and Taulelle, F. (2009). 29Si NMR Relaxation of Silicated Nanoparticles in Tetraethoxysilane–Tetrapropylammonium Hydroxide–Water System (TEOS–TPAOH–H2O). *J. Phys. Chem. C* 113, 10838–10841. doi:10.1021/jp903454f

Henning, L. M., Simon, U., Gurlo, A., Smales, G. J., and Bekheet, M. F. (2019). Grafting and Stabilization of Ordered Mesoporous Silica COK-12 with Graphene Oxide for Enhanced Removal of Methylene Blue. *RSC Adv.* 9, 36271–36284. doi:10.1039/c9ra05541j

Jacobs, P. A. (1987). Chapter I: Synthesis of ZSM-5 Zeolites in the Presence of Tetrapropylammonium Ions. *Stud. Surf. Sci. Catal.* 33, 47–111. doi:10.1016/S0167-2991(09)60467-5

Jammaer, J., Aerts, A., D'Haen, J., Seo, J. W., and Martens, J. A. (2009). Convenient Synthesis of Ordered Mesoporous Silica at Room Temperature and Quasi-Neutral pH. *J. Mater. Chem.* 19, 8290. doi:10.1039/b915273c

Jammaer, J., van Erp, T. S., Aerts, A., Kirschhock, C. E. A., and Martens, J. A. (2011). Continuous Synthesis Process of Hexagonal Nanoplates ofP6mOrdered Mesoporous Silica. *J. Am. Chem. Soc.* 133, 13737–13745. doi:10.1021/ja205627t

Jyothi, Y., ReshmaMurali, K., Murali, K., Shankar, B., Ram Rao, K. S., Raju, B. D., et al. (2017). Mesoporous COK-12 Supported Co3O4 Composites for Adsorption of Methylene Blue from Aqueous Solution. *Asian J. Chem.* 29, 1612–1616. doi:10.14233/ajchem.2017.20616

Kerkhofs, S., Saïdi, F., Vandervoort, N., Van den Mooter, G., Martineau, C., Taulelle, F., et al. (2015a). Silica Capsules Enclosing P123 Triblock Copolymer Micelles for Flurbiprofen Storage and Release. *J. Mater. Chem. B* 3, 3054–3061. doi:10.1039/c5tb00058k

Kerkhofs, S., Willhammar, T., Van Den Noortgate, H., Kirschhock, C. E. A., Breynaert, E., Van Tendeloo, G., et al. (2015b). Self-Assembly of Pluronic F127-Silica Spherical Core-Shell Nanoparticles in Cubic Close-Packed Structures. *Chem. Mater.* 27, 5161–5169. doi:10.1021/acs.chemmater.5b01772

Khan, A. L., Sree, S. P., Martens, J. A., Raza, M. T., and Vankelecom, I. F. J. (2015). Mixed Matrix Membranes Comprising of Matrimid and Mesoporous COK-12: Preparation and Gas Separation Properties. *J. Membr. Sci.* 495, 471–478. doi:10.1016/j.memsci.2015.08.008

Khouw, C. B., Dartt, C. B., Labinger, J. A., and Davis, M. E. (1994). Studies on the Catalytic-Oxidation of Alkanes and Alkenes by Titanium Silicates. *J. Catal.* 149, 195–205. doi:10.1006/jcat.1994.1285

Kim, S.-S., Pauly, T. R., and Pinnavaia, T. J. (2000). Non-ionic Surfactant Assembly of Ordered, Very Large Pore Molecular Sieve Silicas from Water Soluble Silicates. *Chem. Commun.*, 1661–1662. doi:10.1039/b002856h

Kim, S. S., Karkamkar, A., Pinnavaia, T. J., Kruk, M., and Jaroniec, M. (2001). Synthesis and Characterization of Ordered, Very Large Pore MSU-H Silicas Assembled from Water-Soluble Silicates. *J. Phys. Chem. B* 105, 7663–7670. doi:10.1021/jp010773p

Kirschhock, C. E. A., Buschmann, V., Kremer, S., Ravishankar, R., Houssin, C. J. Y., Mojet, B. L., et al. (2001). Zeosil Nanoslabs: Building Blocks innPr4N+-Mediated Synthesis of MFI Zeolite. *Angew. Chem. Int. Ed.* 40, 2637–2640. doi:10.1002/1521-3773(20010716)40:14<2637:aid-anie2637>3.0.co;2-7

Kirschhock, C. E. A., Kremer, S. P. B., Vermant, J., Van Tendeloo, G., Jacobs, P. A., and Martens, J. A. (2005). Design and Synthesis of Hierarchical Materials from Ordered Zeolitic Building Units. *Chem. Eur. J.* 11, 4306–4313. doi:10.1002/chem.200401329

Kirschhock, C. E. A., Ravishankar, R., Jacobs, P. A., and Martens, J. A. (1999a). Aggregation Mechanism of Nanoslabs with Zeolite MFI-type Structure. *J. Phys. Chem. B* 103, 11021–11027. doi:10.1021/jp992272y

Kirschhock, C. E. A., Ravishankar, R., Looveren, L. V., Jacobs, P. A., and Martens, J. A. (1999b). Mechanism of Transformation of Precursors into Nanoslabs in the Early Stages of MFI and MEL Zeolite Formation from TPAOH–TEOS–H2O and TBAOH–TEOS–H2O Mixtures. *J. Phys. Chem. B* 103, 4972–4978. doi:10.1021/jp990298j

Kirschhock, C. E. A., Ravishankar, R., Verspeurt, F., Grobet, P. J., Jacobs, P. A., and Martens, J. A. (1999c). Identification of Precursor Species in the Formation of MFI Zeolite in the TPAOH–TEOS–H2O System. *J. Phys. Chem. B* 103, 4965–4971. doi:10.1021/jp990297r

Kokotailo, G. T., Lawton, S. L., Olson, D. H., and Meier, W. M. (1978). Structure of Synthetic Zeolite ZSM-5. *Nature* 272, 437–438. doi:10.1038/272437a0

Kragten, D. D., Fedeyko, J. M., Sawant, K. R., Rimer, J. D., Vlachos, D. G., Lobo, R. F., et al. (2003). Structure of the Silica Phase Extracted from Silica/(TPA)OH Solutions Containing Nanoparticles. *J. Phys. Chem. B* 107, 10006–10016. doi:10.1021/jp035110h

Kremer, S. P. B., Kirschhock, C. E. A., Aerts, A., Aerts, C. A., Houthoofd, K. J., Grobet, P. J., et al. (2005a). Zeotile-2: A Microporous Analogue of MCM-48. *Solid State. Sci.* 7, 861–867. doi:10.1016/j.solidstatesciences.2005.01.021

Kremer, S. P. B., Kirschhock, C. E. A., Aerts, A., Villani, K., Martens, J. A., Lebedev, O. I., et al. (2003). Tiling Silicalite-1 Nanoslabs into 3D Mosaics. *Adv. Mater.* 15, 1705–1707. doi:10.1002/adma.200305266

Kremer, S. P. B., Kirschhock, C. E. A., Jacobs, P. A., and Martens, J. A. (2005b). Synthesis and Characterization of Zeogrid Molecular Sieves. *Comptes Rendus Chim.* 8, 379–390. doi:10.1016/j.crci.2004.10.015

Kremer, S. P. B., Kirschhock, C. E. A., Tielen, M., Collignon, F., Grobet, P. J., Jacobs, P. A., et al. (2000). Preparation of Zeogrids through Interposed Stapling and Fusion of MFI Zeolite Type Nanoslabs. *Stud. Surf. Sci. Catal.*, 185–192. doi:10.1016/s0167-2991(00)80656-4

Kremer, S. P. B., Kirschhock, C. E. A., Tielen, M., Collignon, F., Grobet, P. J., Jacobs, P. A., et al. (2002). Silicalite-1 Zeogrid: A New Silica Molecular Sieve with Super- and Ultra-micropores. *Adv. Funct. Mater.* 12, 286. doi:10.1002/1616-3028(20020418)12:4<286:aid-adfm286>3.0.co;2-m

Lesthaeghe, D., Vansteenkiste, P., Verstraelen, T., Ghysels, A., Kirschhock, C. E. A., Martens, J. A., et al. (2008). MFI Fingerprint: How Pentasil-Induced IR Bands Shift during Zeolite Nanogrowth. *J. Phys. Chem. C* 112, 9186–9191. doi:10.1021/jp711550s

Liang, D., Follens, L. R. A., Aerts, A., Martens, J. A., Van Tendeloo, G., and Kirschhock, C. E. A. (2007). TEM Observation of Aggregation Steps in Room-Temperature Silicalite-1 Zeolite Formation. *J. Phys. Chem. C* 111, 14283–14285. doi:10.1021/jp074960k

Madon, R. (1991). Role of ZSM-5 and Ultrastable Y Zeolites for Increasing Gasoline Octane Number. *J. Catal.* 129, 275–287. doi:10.1016/0021-9517(91)90030-8

Martens, J. A., and Jacobs, P. A. (1986). The Potential and Limitations of the N-Decane Hydroconversion as a Test Reaction for Characterization of the Void Space of Molecular Sieve Zeolites. *Zeolites* 6, 334–348. doi:10.1016/0144-2449(86)90061-8

Martens, J. A., Parton, R., Uytterhoeven, L., Jacobs, P. A., and Froment, G. F. (1991). Selective Conversion of Decane into Branched Isomers. *Appl. Catal.* 76, 95–116. doi:10.1016/0166-9834(91)80007-j

Martens, J. A., Souverijns, W., Verrelst, W., Parton, R., Froment, G. F., and Jacobs, P. A. (1995). Selective Isomerization of Hydrocarbon Chains on External Surfaces of Zeolite Crystals. *Angew. Chem. Int. Ed. Engl.* 34, 2528–2530. doi:10.1002/anie.199525281

Martens, J. A., Thybaut, J. W., Denayer, J. F. M., Sree, S. P., Aerts, A., Reyniers, M.-F., et al. (2011). Catalytic and Molecular Separation Properties of Zeogrids and Zeotiles. *Catal. Today* 168, 17–27. doi:10.1016/j.cattod.2011.01.036

Martens, J. A., Tielen, M., Jacobs, P. A., and Weitkamp, J. (1984). Estimation of the Void Structure and Pore Dimensions of Molecular Sieve Zeolites Using the Hydroconversion of N-Decane. *Zeolites* 4, 98–107. doi:10.1016/0144-2449(84)90044-7

Martens, J. A., Vanbutsele, G., Jacobs, P. A., Denayer, J., Ocakoglu, R., Baron, G., et al. (2001). Evidences for Pore Mouth and Key-Lock Catalysis in Hydroisomerization of Long N-Alkanes over 10-ring Tubular Pore Bifunctional Zeolites. *Catal. Today* 65, 111–116. doi:10.1016/s0920-5861(00)00577-0

Mellaerts, R., Aerts, C. A., Humbeeck, J. V., Augustijns, P., den Mooter, G. V., and Martens, J. A. (2007). Enhanced Release of Itraconazole from Ordered Mesoporous SBA-15 Silica Materials. *Chem. Commun.* 1375, 1375. doi:10.1039/b616746b

Morais, A. F., Silva, I. G. N., Sree, S. P., de Melo, F. M., Brabants, G., Brito, H. F., et al. (2017). Hierarchical Self-Supported ZnAlEu LDH Nanotubes Hosting Luminescent CdTe Quantum Dots. *Chem. Commun.* 53, 7341–7344. doi:10.1039/c7cc02097j

Mustafa, D., Breynaert, E., Bajpe, S. R., Martens, J. A., and Kirschhock, C. E. A. (2011). Stability Improvement of Cu3(BTC)2 Metal–Organic Frameworks under Steaming Conditions by Encapsulation of a Keggin Polyoxometalate. *Chem. Commun.* 47, 8037. doi:10.1039/c1cc12341f

Mustafa, D., Silva, I. G. N., Bajpe, S. R., Martens, J. A., Kirschhock, C. E. A., Breynaert, E., et al. (2014). Eu@COK-16, a Host Sensitized, Hybrid Luminescent Metal–Organic Framework. *Dalton Trans.* 43, 13480–13484. doi:10.1039/c4dt00899e

Persson, A. E., Schoeman, B. J., Sterte, J., and Otterstedt, J.-E. (1994). The Synthesis of Discrete Colloidal Particles of TPA-Silicalite-1. *Zeolites* 14, 557–567. doi:10.1016/0144-2449(94)90191-0

Pochamoni, R., Narani, A., Gurram, V. R. B., Gudimella, M. D., Sai Prasad Potharaju, P. S., Burri, D. R., et al. (2014). Molybdenum Oxide Supported on COK-12: A Novel Catalyst for Oxidative Dehydrogenation of Ethylbenzene Using CO2. *Indian J. Chem. - Sect. A. Inorganic, Phys. Theor. Anal. Chem.* 53, 493–498.

Pochamoni, R., Narani, A., Varkolu, M., Dhar Gudimella, M., Prasad Potharaju, S. S., Burri, D. R., et al. (2015). Studies on Ethylbenzene Dehydrogenation with CO2 as Soft Oxidant over Co3O4/COK-12 Catalysts. *J. Chem. Sci.* 127, 701–709. doi:10.1007/s12039-015-0826-x

Pulinthanathu Sree, S., Dendooven, J., Geerts, L., Ramachandran, R. K., Javon, E., Ceyssens, F., et al. (2017). 3D Porous Nanostructured Platinum Prepared Using Atomic Layer Deposition. *J. Mater. Chem. A.* 5, 19007–19016. doi:10.1039/c7ta03257a

Pulinthanathu Sree, S., Dendooven, J., Jammaer, J., Masschaele, K., Deduytsche, D., D'Haen, J., et al. (2012). Anisotropic Atomic Layer Deposition Profiles of TiO2 in Hierarchical Silica Material with Multiple Porosity. *Chem. Mater.* 24, 2775–2780. doi:10.1021/cm301205p

Qiu, L.-G., Xu, T., Li, Z.-Q., Wang, W., Wu, Y., Jiang, X., et al. (2008). Hierarchically Micro- and Mesoporous Metal–Organic Frameworks with Tunable Porosity. *Angew. Chem. Int. Ed.* 47, 9487–9491. doi:10.1002/anie.200803640

Ramanan, H., Kokkoli, E., and Tsapatsis, M. (2004). On the TEM and AFM Evidence of Zeosil Nanoslabs Present during the Synthesis of Silicalite-1. *Angew. Chem. Int. Ed.* 43, 4558–4561. doi:10.1002/anie.200460376

Ravishankar, R., Kirschhock, C. E. A., Knops-Gerrits, P.-P., Feijen, E. J. P., Grobet, P. J., Vanoppen, P., et al. (1999). Characterization of Nanosized Material Extracted from Clear Suspensions for MFI Zeolite Synthesis. *J. Phys. Chem. B* 103, 4960–4964. doi:10.1021/jp990296z

Ravishankar, R., Kirschhock, C., Schoeman, B. J., Vanoppen, P., Grobet, P. J., Storck, S., et al. (1998). Physicochemical Characterization of Silicalite-1 Nanophase Material. *J. Phys. Chem. B* 102, 2633–2639. doi:10.1021/jp973147u

Reichinger, M., Schmidt, W., Berg, M. W. E. v. d., Aerts, A., Martens, J. A., Kirschhock, C. E. A., et al. (2010). Alkene Epoxidation with Mesoporous Materials Assembled from TS-1 Seeds - Is There a Hierarchical Pore System? *J. Catal.* 269, 367–375. doi:10.1016/j.jcat.2009.11.023

Rimer, J. D., Vlachos, D. G., and Lobo, R. F. (2005). Evolution of Self-Assembled Silica–Tetrapropylammonium Nanoparticles at Elevated Temperatures. *J. Phys. Chem. B* 109, 12762–12771. doi:10.1021/jp052045y

Schoeman, B. J., and Regev, O. (1996). A Study of the Initial Stage in the Crystallization of TPA-Silicalite-1. *Zeolites* 17, 447–456. doi:10.1016/s0144-2449(96)00038-3

Souverijns, W., Verrelst, W., Vanbutsele, G., Martens, J. A., and Jacobs, P. A. (1994). Micropore Structure of Zeolite MCM-22 as Determined by the Decane Catalytic Test Reaction. *J. Chem. Soc. Chem. Commun.*, 1671. doi:10.1039/c39940001671

Speybroeck, M. V., Barillaro, V., Thi, T. D., Mellaerts, R., Martens, J., Humbeeck, J. V., et al. (2009). Ordered Mesoporous Silica Material SBA-15: A Broad-Spectrum Formulation Platform for Poorly Soluble Drugs. *J. Pharm. Sci.* 98, 2648–2658. doi:10.1002/jps.21638

Sree, S. P., Dendooven, J., Masschaele, K., Hamed, H. M., Deng, S., Bals, S., et al. (2013). Synthesis of Uniformly Dispersed Anatase Nanoparticles inside Mesoporous Silica Thin Films *via* Controlled Breakup and Crystallization of Amorphous TiO2 Deposited Using Atomic Layer Deposition. *Nanoscale* 5, 5001. doi:10.1039/c3nr00594a

Sree, S. P., Dendooven, J., Smeets, D., Deduytsche, D., Aerts, A., Vanstreels, K., et al. (2011). Spacious and Mechanically Flexible Mesoporous Silica Thin Film Composed of an Open Network of Interlinked Nanoslabs. *J. Mater. Chem.* 21, 7692. doi:10.1039/c1jm10270b

Srinivas, D., Srivastava, R., and Ratnasamy, P. (2004). Transesterifications over Titanosilicate Molecular Sieves. *Catal. Today* 96, 127–133. doi:10.1016/j.cattod.2004.06.113

Sun, L.-B., Li, J.-R., Park, J., and Zhou, H.-C. (2011). Cooperative Template-Directed Assembly of Mesoporous Metal–Organic Frameworks. *J. Am. Chem. Soc.* 134, 126–129. doi:10.1021/ja209698f

Tiseanu, C., Gessner, A., Kumke, M., Gagea, B., Parvulescu, V. I., and Martens, J. (2008a). Photoluminescence Spectra and Dynamics of Lanthanide-Doped Microporous-Mesoporous Materials. *J. Lumin.* 128, 751–753. doi:10.1016/j.jlumin.2007.10.018

Tiseanu, C., Geßner, A., and Kumke, M. U. (2008b). Dehydration and Rehydration Effects on the Photoluminescence Properties of Terbium-Exchanged MFI-type Materials. *J. Non-Crystalline Sol.* 354, 1969–1975. doi:10.1016/j.jnoncrysol.2007.11.017

Tiseanu, C., Kumke, M. U., Parvulescu, V. I., Gessner, A., Gagea, B. C., and Martens, J. A. (2006). Photoluminescence Response of Terbium-Exchanged MFI-type Materials to Si/Al Ratio, Texture, and Hydration State. *J. Phys. Chem. B* 110, 25707–25715. doi:10.1021/jp0636827

Tiseanu, C., Kumke, M. U., Parvulescu, V. I., Gessner, A., Gagea, B., and Martens, J. (2008c). Europium(3+): An Efficient Luminescence Probe for the Si to Al Ratio and Silylation Effects in the Microporous–Mesoporous Zeogrid Materials. *J. Phys. Chem. B* 112, 10552–10562. doi:10.1021/jp711337h

Tiseanu, C., Kumke, M. U., Parvulescu, V. I., and Martens, J. (2009). Species-related Luminescence-Structure Relationships in Europium-Exchanged Mesoporous Material. *J. Appl. Phys.* 105, 063521. doi:10.1063/1.3086634

Van Borm, R., Aerts, A., Reyniers, M.-F., Martens, J. A., and Marin, G. B. (2010). Catalytic Cracking of 2,2,4-Trimethylpentane on FAU, MFI, and Bimodal Porous Materials: Influence of Acid Properties and Pore Topology. *Ind. Eng. Chem. Res.* 49, 6815–6823. doi:10.1021/ie901708m

Verheyen, E., Jo, C., Kurttepeli, M., Vanbutsele, G., Gobechiya, E., Korányi, T. I., et al. (2013). Molecular Shape-Selectivity of MFI Zeolite Nanosheets in N-Decane Isomerization and Hydrocracking. *J. Catal.* 300, 70–80. doi:10.1016/j.jcat.2012.12.017

Vialpando, M., Aerts, A., Persoons, J., Martens, J., and Van Den Mooter, G. (2011a). Evaluation of Ordered Mesoporous Silica as a Carrier for Poorly Soluble Drugs: Influence of Pressure on the Structure and Drug Release. *J. Pharm. Sci.* 100, 3411–3420. doi:10.1002/jps.22535

Vialpando, M., Martens, J. A., and Van den Mooter, G. (2011b). Potential of Ordered Mesoporous Silica for Oral Delivery of Poorly Soluble Drugs. *Ther. Deliv.* 2, 1079–1091. doi:10.4155/tde.11.66

Wee, L. H., Meledina, M., Turner, S., Custers, K., Kerkhofs, S., Sree, S. P., et al. (2016). Anatase TiO2 Nanoparticle Coating on Porous COK-12 Platelets as Highly Active and Reusable Photocatalysts. *RSC Adv.* 6, 46678–46685. doi:10.1039/c6ra06141a

Wee, L. H., Meledina, M., Turner, S., Custers, K., Kerkhofs, S., van Tendeloo, G., et al. (2015). Hematite Iron Oxide Nanorod Patterning inside COK-12 Mesochannels as an Efficient Visible Light Photocatalyst. *J. Mater. Chem. A.* 3, 19884–19891. doi:10.1039/c5ta05075h

Wee, L. H., Meledina, M., Turner, S., Van Tendeloo, G., Zhang, K., Rodriguez-Albelo, L. M., et al. (2017). 1D-2D-3D Transformation Synthesis of Hierarchical Metal–Organic Framework Adsorbent for Multicomponent Alkane Separation. *J. Am. Chem. Soc.* 139, 819–828. doi:10.1021/jacs.6b10768

Wee, L. H., Wiktor, C., Turner, S., Vanderlinden, W., Janssens, N., Bajpe, S. R., et al. (2012). Copper Benzene Tricarboxylate Metal–Organic Framework with Wide Permanent Mesopores Stabilized by Keggin Polyoxometallate Ions. *J. Am. Chem. Soc.* 134, 10911–10919. doi:10.1021/ja302089w

Yebo, N. A., Sree, S. P., Levrau, E., Detavernier, C., Hens, Z., Martens, J. A., et al. (2012). Selective and Reversible Ammonia Gas Detection with Nanoporous Film Functionalized Silicon Photonic Micro-ring Resonator. *Opt. Express* 20, 11855. doi:10.1364/oe.20.011855

Zhao, D., Feng, J., Huo, Q., Melosh, N., Fredrickson, G. H., Chmelka, B. F., et al. (1998). Triblock Copolymer Syntheses of Mesoporous Silica with Periodic 50 to 300 Angstrom Pores. *Science* 279, 548–552. doi:10.1126/science.279.5350.548

Conflict of Interest: The authors declare that the research was conducted in the absence of any commercial or financial relationships that could be construed as a potential conflict of interest.

Publisher's Note: All claims expressed in this article are solely those of the authors and do not necessarily represent those of their affiliated organizations, or those of the publisher, the editors, and the reviewers. Any product that may be evaluated in this article, or claim that may be made by its manufacturer, is not guaranteed or endorsed by the publisher.